Journal of Engineering Mathematics (2025) 153:7
https://doi.org/10.1007/s10665-025-10469-0

Design optimization with complex-valued material parameters

Ursula Weiss[2] · **Malte A. Peter**[1,2]

Received: 12 December 2024 / Accepted: 7 July 2025

Abstract
We consider the two-phase design optimization problem for a linear scalar second-order elliptic equation with complex-valued material parameters modeling dielectric and conductive properties in time-harmonic electrostatics as they arise, e.g., in sensor design optimization. Owing to the complex-valued material parameters, application of well-established topology optimization theory is not directly possible. We discuss obstacles and limitations of the relaxation via homogenization method in this context and derive a gradient descent method based on restriction of admissible designs to simple laminates. Numerical simulations showcase the functioning of the method for optimizing the design of an electric field sensor.

Keywords Homogenization · Relaxation · Sensor optimization · Time-harmonic electrostatics · Topology optimization

Mathematics Subject Classification 49J45 · 49K20 · 78M40 · 35B27

1 Introduction

In the early stage of design, when all aspects such as sizing, shape, and topology of a structure are of general interest and can significantly affect its performance, topology optimization approaches are popular for design optimization [1, 2]. If the design to be optimized is that of a sensor for electromagnetic waves, e.g., its optimal position, shape, and size, the underlying field equations are those describing electromagnetic wave propagation, which, when considered in the time-harmonic setting, are complex-

✉ Ursula Weiss
ursula.weiss@uni-a.de

Malte A. Peter
malte.peter@uni-a.de

1 Institute of Mathematics, University of Augsburg, Universitätsstraße 12a, 86159 Augsburg, Germany

2 Centre for Advanced Analytics and Predictive Sciences, University of Augsburg, Universitätsstraße 12a, 86159 Augsburg, Germany

Published online: 01 August 2025

valued, and so are the material parameters. In contrast to well-known design problems based on materials with real-valued material parameters, the case of materials with complex-valued material parameters seems to have remained undeveloped thus far.

In general, topology optimization problems can be formulated as two-phase optimization problems in which a fixed proportion of two different materials (for example, air and copper) is distributed in a given domain in such a way that a given objective functional (for example, the energy captured by the sensor made of copper) is maximized. The objective functional depends on the solution of an underlying state equation modeling the physics in the considered domain (for example the equations of electrostatics). The so-called 0–1-formulation of the optimization problem determines for every point in the physical design domain if there is material (1) or not (0) or, alternatively, if there is material A (1) or B (0). In absence of any additional constraints such as perimeter constraints limiting the perimeter of the derived shape, a minimal length scale, or a maximum number of components, optimization problems in this formulation usually do not admit solutions in the set of desired admissible 0–1-designs [3]. For example, a structure with many tiny inclusions of one material often has better properties than a structure with few larger inclusions of the same total volume. A proposed design can therefore be improved by making further variations of the phase arrangement, i.e., an increasingly finer mixture of the two materials leading to a composite material. This illustrates that optimal design problems in 0–1-formulation are not inherently well posed and in general do not admit classical design solutions (0–1-solutions) [3].

There are different options to overcome this issue leading to a well-posed optimization problem, which involve the introduction of a material density instead of dealing with discrete values 0 and 1 (see, for example, [4]). In so-called relaxation approaches, which are considered in what follows, the set of admissible designs in the 0–1-formulation, containing the two pure materials A and B, is extended (relaxed) to an appropriate closure of the space of admissible designs, allowing for the above-mentioned composite materials consisting of materials A and B with their effective material properties as admissible design materials.

In the context of physics based on scalar second-order elliptic equations with real-valued material parameters, the theory of homogenization and, particularly, H-convergence [5] forms the basis for this relaxation procedure, as it allows to characterize the composite materials obtained by the closure of the space of admissible designs. This enables the derivation of necessary optimality conditions, once the well-posed relaxed problem setting is derived. If necessary, a penalization process to regain a 0–1-formulation can be applied once the optimal design in the relaxed admissible set is found. In [3], Allaire gives a comprehensive exposition of the theory of shape optimization via homogenization for real-valued material parameters.

The present paper extends this theory to design optimization in the context of single-frequency time-harmonic electromagnetic wave propagation. In what follows, we show that the generic optimal sensor shape optimization problem can in fact be modeled based on a scalar second-order elliptic equation expressing electrostatics in the frequency domain. However, the mathematical formulation of the described problem as an optimal design problem in 0–1-formulation reveals that the theory of shape optimization via homogenization must be extended to allow for complex-valued

material parameters. We discuss how this can be done based on the assumption that the closure of the space of admissible designs is characterized in an analogous way as in the real-valued case and we point to the open mathematical questions in this context. Moreover, it turns out that, for complex-valued material parameters, the derivation of optimality criteria following the relaxation procedure is not straightforward and we overcome this problem using Wirtinger calculus. As a result, under certain restrictions and assumptions, discussed and outlined below, we derive an optimization method successfully optimizing the design of the electromagnetic sensor, which we illustrate by means of a numerical example.

This article is organized as follows. In Sect. 2, we derive a formulation of the underlying partial differential equation modeling time-harmonic electrostatics in dielectric and conductive media, in which the design materials are completely represented by (complex-valued) material parameters. Based on this, Sect. 3 contains the formulation of the optimal design problem of shape optimization with complex-valued material parameters. In Sect. 4, we aim for a relaxation approach as described by Allaire in [3] and point out the obstacles and limitations when dealing with complex-valued material parameters. Making certain assumptions on the relaxed admissible design set, we then derive the Gâteaux differential of the objective functional and a gradient descent method based on the restriction of the admissible design set to simple laminates. Section 5 demonstrates the functionality of this approach. A short conclusion is given in Sect. 6.

2 Electrostatics in materials with both dielectric and conductive properties

In order to state the problem in a way amenable to optimization via homogenization, we require a formulation such that the design materials are completely represented in terms of material parameters in the state equation. Therefore, we begin by deriving a formulation of time-harmonic electrostatics in a material where all effects (including conduction) are condensed in a single complex material parameter, which may be useful in other contexts as well.

Following the argumentation in [6], the macroscopic Gauß law is given by

$$\operatorname{div}(\epsilon_0 \mathcal{E}) = \rho_{\text{ext}} + \rho_{\text{c}} + \rho_{\text{b}}, \tag{1}$$

where $\mathcal{E}$ is the (real-valued) electric field, ϵ_0 is the electric constant, ρ_{b} is the charge density arising from charge carriers bound in the material, and ρ_{c} and ρ_{ext} are densities contributed by free charge carriers of the material and charge carriers introduced into the system from external sources, respectively. In the context of what follows, a typical example for an external source is the source to be detected by the sensor.

In Sects. 2.1 and 2.2, we briefly show how to encode the effect of ρ_{b} and ρ_{c} in a combined (frequency-dependent) material parameter in front of $\mathcal{E}$ in Eq. (1) in the time-harmonic setting.

2.1 Dielectric effects

An external electric field applied to a dielectric material shifts bound charges on the atomic or molecular scale, forming electric dipoles. Polarization $\mathcal{P}$, the average dipole charge density, takes these effects into account on the macroscopic level via

$$\rho_{\mathrm{b}} = -\operatorname{div} \mathcal{P}.$$

Assuming homogeneous isotropic linear dielectric materials, polarization is proportional to the electric field with factor of proportionality χ_{e}, which is known as the electrical susceptibility of the material. Taking into account that the response of the medium to the applied electric field is not instantaneous, this leads to

$$\mathcal{P}(t) = \epsilon_0 \int_{-\infty}^{t} \chi_{\mathrm{e}}(t - t')\mathcal{E}(t')\,\mathrm{d}t',$$

or, in the frequency domain, i.e., $\mathcal{E} = \mathbb{R}\mathrm{e}\{E\mathrm{e}^{-\mathrm{i}\omega t}\}$ and $\mathcal{P} = \mathbb{R}\mathrm{e}\{P\mathrm{e}^{-\mathrm{i}\omega t}\}$ with complex-valued spatial parts of the potential, E, and polarization, P, respectively, to

$$P = \epsilon_0 \chi_{\mathrm{e}}(\omega) E.$$

Accordingly, Eq. (1) becomes

$$\operatorname{div}(\epsilon_0(1 + \chi_{\mathrm{e}}(\omega))E) = \rho_{\mathrm{ext}} + \rho_{\mathrm{c}}. \tag{2}$$

The function $1 + \chi_{\mathrm{e}}(\omega)$ describing the properties of the material due to bound charges is often subsumed as relative electric permittivity $\epsilon_{\mathrm{r}}(\omega) := 1 + \chi_{\mathrm{e}}(\omega)$, so that (2) is typically written as

$$\operatorname{div}(\epsilon_0 \epsilon_{\mathrm{r}}(\omega) E) = \rho_{\mathrm{ext}} + \rho_{\mathrm{c}}. \tag{3}$$

In general, ϵ_{r} is complex-valued, i.e., $\epsilon_{\mathrm{r}} = \epsilon_{\mathrm{p}}' + \mathrm{i}\epsilon_{\mathrm{p}}''$, accounting for refraction (real part) and absorption (imaginary part) of the propagating electromagnetic wave in the dielectric material due to polarization effects [7]. In order to examine the behavior of the material parameter ϵ_r more concretely, a simplified model of the motion of bound electrons in the presence of an applied field (see for example [6–8]) can be considered. Considering harmonically oscillating electric fields with frequency ω in materials with bound electrons, it is possible to deduce from this simple model the relative permittivity as

$$\epsilon_{\mathrm{r}}(\omega) = 1 + \frac{\omega_{\mathrm{p}}^2}{\omega_0^2 - \omega^2 - \mathrm{i}\omega\gamma}$$

with $\omega_\mathrm{p} = \frac{N_\mathrm{b} e^2}{\epsilon_0 m}$, the so-called plasma frequency, ω_0 the resonance frequency and γ the collision rate of the material. In the definition of ω_p, the quantities N_b, e and m are the volume density of electrons, electric charge and mass of an electron, respectively.

This model describing the relative permittivity is usually called Lorentz-oscillator model (cf. [6]) or Lorentz dielectric (cf. [7]).

2.2 Conduction effects

Free charge carriers of conductive materials subjected to an external electric field contribute to the free charge density via ρ_c. The time-varying charge density $\rho_\mathrm{c}(t)$ is the source for a related current $\mathcal{J}_\mathrm{c}$. Considering the associated conservation equation

$$\frac{\mathrm{d}}{\mathrm{d}t}\rho_\mathrm{c}(t) = -\operatorname{div}\mathcal{J}_\mathrm{c}(t)$$

leads to

$$(-\mathrm{i}\omega)\rho_\mathrm{c} = -\operatorname{div} J_\mathrm{c}$$

in the frequency domain (with obvious notations for the time-harmonic quantities). Applying Ohm's law, $J_\mathrm{c} = \sigma E$, in the deduced equation gives

$$\rho_\mathrm{c} = \operatorname{div}\left(\frac{1}{\mathrm{i}\omega}\sigma(\omega)E\right) \tag{4}$$

with complex-valued frequency-dependent conductivity $\sigma(\omega)$.

Considering again harmonic oscillating fields with frequency ω, it is possible to deduce the conductivity as

$$\sigma(\omega) = \frac{\epsilon_0\omega_\mathrm{p}^2}{\gamma - \mathrm{i}\omega}$$

with plasma frequency $\omega_\mathrm{p} = \frac{N_\mathrm{b} e^2}{\epsilon_0 m}$ as before, which is known as the Drude model [7].

Substituting (4) in (3), we obtain Gauß's law in general media with bound and unbound charge carriers,

$$\operatorname{div}\left(\epsilon_0 + \epsilon_0\chi_\mathrm{e}(\omega) - \frac{1}{\mathrm{i}\omega}\sigma(\omega)E\right) = \rho_\mathrm{ext}. \tag{5}$$

Combining further the polarization and conductive effects of materials in one generalized complex-valued material parameter $\epsilon = \epsilon' + \mathrm{i}\epsilon''$, called the total effective permittivity [7],

$$\epsilon(\omega) = \epsilon_0 + \epsilon_0\chi_\mathrm{e}(\omega) - \frac{1}{\mathrm{i}\omega}\sigma(\omega),$$

leads to

$$\operatorname{div}(\epsilon(\omega)E) = \rho_{\text{ext}}. \tag{6}$$

Equations (5) and (6) describe the propagation of the electric field in general media with bound and unbound charge carriers. The real part of the total effective permittivity leads to refraction, the imaginary part to absorption of the electromagnetic wave in the material. As described above, the material parameter ϵ combines properties of the material due to bound and unbound charge carriers in the material. For frequencies $\omega \neq 0$, the real and imaginary parts account for refraction and absorption of the electromagnetic waves, but since both, real and imaginary part, generally consist of the two components arising from bound and unbound charge carriers they do not allow a direct interpretation as dielectric properties or conductivity of the material. A direct connection between conductivity of the material and the imaginary part of the material parameter can only be established for the low-frequency limit $\omega \to 0$.

2.3 Equations of electrostatics in general media

In what follows, the time-harmonic case for low frequencies ω is considered and inductive effects are neglected in the model. Thus, the electric field (in a simply connected domain) can be expressed as the gradient of a scalar electric potential V,

$$E(x) = -\nabla V(x).$$

Together with Eq. (6), this leads to the following complex-valued single equation to be solved for V for given frequency ω:

$$-\operatorname{div}(\epsilon(\omega)\nabla V(x)) = \rho_{\text{ext}}. \tag{7}$$

As described above, the parameter ϵ summarizes the contributions due to bound and unbound charge carriers in the material. Any external source enters the equation via ρ_{ext}. These equations of electrostatics in general media represent the state equation and provide the basis for consideration of the described optimal design problem as a two-phase optimization problem in the context of the homogenization method. The effects of dielectric and conductive properties of the materials are included by a complex-valued material constant without any additional boundary conditions.

3 The shape optimization problem

Based on the derived formulation of the underlying partial differential Eq. (7) modeling the physics, the problem formulation with real-valued material parameters presented in [3] is adapted. In what follows, the well-known case with material parameters in $\mathbb{R}$ is termed real-valued parameter case, the case relevant here with material parameters in $\mathbb{C}$ as complex-valued parameter case. In the design problem, the optimal distribution of two isotropic materials A and B of fixed volume in a given open bounded Lipschitz

domain $\Omega \subset \mathbb{R}^N$ is sought, such that a given criterion, which depends on the solution of the deduced underlying state equation in Ω, is minimized, i.e., the distribution of the two materials A and B with constant isotropic material parameters $\epsilon_\alpha(\omega) = \alpha = \alpha_\mathrm{r} + \mathrm{i}\alpha_\mathrm{i}$ and $\epsilon_\beta(\omega) = \beta = \beta_\mathrm{r} + \mathrm{i}\beta_\mathrm{i}$, $\alpha, \beta \in \mathbb{C}$ in Ω for fixed (low) frequency ω is to be found. We assume $\alpha_\mathrm{r}, \beta_\mathrm{r} > 0$ and $\alpha_\mathrm{i}, \beta_\mathrm{i} \geq 0$ in order to set up a physically natural problem (avoiding the need for metamaterials).

The characteristic function

$$\chi(x) = \begin{cases} 1 & \text{if phase A is present at point } x, \\ 0 & \text{if phase B is present at point } x, \end{cases}$$

defines the part of Ω occupied by phase A and the overall material parameter is accordingly formulated as

$$a_\chi = \alpha\chi + \beta(1 - \chi).$$

In view of (7), the state equation of the optimization problem models the electric potential u_χ in the domain Ω and is given by

$$\begin{cases} -\mathrm{div}(a_\chi(x)\nabla u_\chi(x)) = f(x), & x \in \Omega, \\ u_\chi(x) = 0, & x \in \partial\Omega, \end{cases} \tag{8}$$

where u_χ is the unknown complex-valued potential, f a given source term in Ω, scalar and independent of χ, and the materials A and B are perfectly electrically bonding. Provided that the source term f belongs to $H^{-1}(\Omega)$, the dual space of the Sobolev space $H_0^1(\Omega)$ of square-integrable functions with square-integrable weak derivatives and vanishing boundary trace, the standard weak form of (8) admits a unique (weak) solution u_χ in $H_0^1(\Omega)$. It is assumed further that the amount of material A is limited by a prescribed volume V_α of A, $0 \leq V_\alpha \leq |\Omega|$, where $|\Omega|$ denotes the measure (volume) of Ω. An admissible design is therefore a function χ such that

$$\chi \in L^\infty(\Omega; \{0, 1\}) \text{ and } \int_\Omega \chi(x)\,\mathrm{d}x = V_\alpha.$$

Denoting the set of admissible configurations by U_ad,

$$U_\mathrm{ad} = \left\{ \chi \in L^\infty(\Omega; \{0, 1\}) \,\middle|\, \int_\Omega \chi(x)\,\mathrm{d}x = V_\alpha \right\}, \tag{9}$$

the objective functional is universally formulated as

$$J(\chi) = \int_\Omega \chi(x) g_\alpha(x, u_\chi(x), \bar{u}_\chi(x)) + (1 - \chi(x)) g_\beta(x, u_\chi(x), \bar{u}_\chi(x))\,\mathrm{d}x,$$

where the overbar denotes complex conjugation and g_α and g_β satisfy certain conditions, namely Carathéodory conditions and growth conditions:

$$\begin{cases} g_{\alpha,\beta}(x,\lambda) \text{ is measurable in } x \text{ for each fixed } \lambda \in \mathbb{C}, \\ g_{\alpha,\beta}(x,\lambda) \text{ is continuous in } \lambda \text{ for a.e. } x \in \Omega, \\ |g_{\alpha,\beta}(x,\lambda)| \leq k(x) + C|\lambda|^m \text{ with } k \in L^1(\Omega),\ 1 \leq m < \frac{2N}{N-2}. \end{cases}$$

Careful consideration of the proof of continuity of Nemytskii operators in [9], using Lebesgue's dominated convergence theorem, which is formulated in $\mathbb{C}$ in [10], confirms that the properties of $g_{\alpha,\beta}$ described in [3] as required in the real-valued parameter case are required in the same way for the complex-valued parameter case to ensure the well posedness of the subsequently derived relaxed optimization problem. Furthermore, it has to be noted that g_α and g_β do not only depend on the solution u_χ of the state equation but also on its complex conjugate $\bar{u}_\chi$. As the objective functional J is commonly a real-valued function depending on the complex-valued u, it is also implicitly dependent on $\bar{u}$. For example, the objective functional considered in the application in Sect. 5,

$$J(\chi) = \int_\Omega \chi(x)|u_\chi(x)|^2 \,\mathrm{d}x,$$

a proxy for the energy captured at a sensor made of material A, must be understood as follows: the function g_β is interpreted depending on x, u_χ and additionally on $\bar{u}_\chi$ with

$$g_\alpha(x,u(x)) = |u_\chi(x)|^2 = u(x)\bar{u}(x) = g_\alpha(x,u_\chi(x),\bar{u}_\chi(x)).$$

Following the general procedure of eliminating constraints in the calculus of variations [11], a Lagrange multiplier $l \in \mathbb{R}$ is introduced in the objective functional instead of enforcing the volume constraint $\int_\Omega \chi(x)\,\mathrm{d}x = V_\alpha$ in the set of admissible designs. For any value of l, there is a corresponding volume constraint such that the optimization problems are equivalent. Even if the converse statement is generally not clear, the optimization routine can be coupled with a bisection method to update the Lagrange multiplier to ensure the compliance with the volume constraint in practice [3]. The complete formulation of the optimal design problem is then stated as follows.
Find $\tilde{\chi}$ such that

$$\tilde{\chi} = \underset{\chi \in U_{\mathrm{ad}}}{\arg\inf}\, J(\chi), \tag{10a}$$

where the real-valued objective functional J is defined by

$$\begin{aligned} J(\chi) = &\int_\Omega \chi(x) g_\alpha(x,u_\chi(x),\bar{u}_\chi(x)) \\ &+(1-\chi(x)) g_\beta(x,u_\chi(x),\bar{u}_\chi(x))\mathrm{d}x + l\int_\Omega \theta(x)\mathrm{d}x \end{aligned} \tag{10b}$$

and u_χ is the (weak) solution of the state equation

$$\begin{cases} -\mathrm{div}(a_\chi(x)\nabla u_\chi(x)) = f(x), & x \in \Omega, \\ u_\chi(x) = 0, & x \in \partial\Omega. \end{cases} \tag{10c}$$

4 Relaxation via homogenization for complex-valued material parameters

Having the model formulation at hand, we now turn to the problem of finding the optimal material distribution expressed in terms of the characteristic function χ. Our approach is based on relaxation via homogenization, the general concept of which we briefly summarize first (e.g., see the monograph [3]).

Considering the optimization problem (10) for material parameters in $\mathbb{R}$ or $\mathbb{C}$, minimizing sequences of designs described by characteristic functions χ may converge to non-classical designs, i.e., the described optimization problem is ill-posed and does not admit a solution in the set of admissible designs (9). To overcome this problem, the idea of relaxation by homogenization is to enlarge the set of admissible designs by allowing for composite materials with their effective macroscopic material parameters deduced by the homogenization process. The mathematical principle of this process is to study the behavior of admissible minimizing sequences and to define so-called generalized or composite admissible designs that include their possible limits. By means of the theory of H-convergence (see [12]), the pairs (θ, A^*) are identified as composite admissible designs relaxing the strict partition induced by χ. The density $\theta \in L^\infty(\Omega; [0, 1])$ describes the local volume ratio between the two phases and A^* is the homogenized tensor of a two-phase composite material obtained by mixing phases A and B in proportions θ and $1 - \theta$ with a microstructure defined by the minimizing sequence. In order to proceed with deriving optimality criteria, it is necessary to characterize the set of all possible homogenized tensors associated with the density θ, which is denoted by $\mathcal{G}_\theta$ and is defined as the closure of $\{A, B\}$ under H-convergence (or G-convergence, which corresponds to H-convergence for symmetric operators).

In general, there are only few examples for which this G-closure problem is solved explicitly. In the case of real-valued material parameters and a scalar second-order elliptic equation, an explicit characterization of $\mathcal{G}_\theta$ and, thus, of the set of generalized designs is available (see for example [13]). In 2d, the optimal geometries, i.e., the composite materials with effective tensors on the boundary of $\mathcal{G}_\theta$, are those of sequential laminates, see the monograph [14]. The derivation of optimality criteria from the corresponding directional derivative of the relaxed objective functional, which is based on the density θ instead of the characteristic function χ, in this case reveals that it is possible to restrict the class of tensors of interest for the optimization to that of rank-1 laminates, which are explicitly characterized by the density θ and lamination direction e (see [3] for a comprehensive summary of the relevant aspects). In what follows, this fact is referred to as optimality of simple laminates. An optimization routine via optimality criteria as well as a gradient descent method can then be formulated based on the design variables θ and e.

In the case of complex-valued material parameters, the general characterization of the G-closure is unknown. Nevertheless, some partial results are available and assuming similar results as in the real-valued case still hold allows to derive a corresponding optimization routine.

4.1 Relaxed admissible design set, adapted problem formulation

The starting point for an application to the complex-valued parameter case along the lines of the argumentation above would be an explicit characterization of the set of admissible homogenized tensors, i.e., the set of composite designs, which boils down to solving the G-closure problem, i.e., to characterize the set $\mathcal{G}_\theta$ in terms of coupled bounds. This is linked with characterization of the micro-geometries, which correspond to the optimal bounds of $\mathcal{G}_\theta$ for complex-valued material parameters. In [15], it is argued that these microstructures are most probably the best candidates for use in structural design. As stated above, this problem has not been comprehensively solved in general but partial results exist.

In [16], it is pointed out that the G-closure problem for complex conductivity is similar to the problem of coupled bounds for two conductivities with the difference that the initial equations are coupled. Furthermore, it is stated that the problem is very similar to the problem addressed in [17, 18] and a derivation can most probably be made along the lines of this work. Apart from improvement of aforementioned bounds, to the best of the authors' knowledge, no one has obtained an explicit characterization of the G-closure of two isotropic phases $\alpha, \beta \in \mathbb{C}$ – even in 2d. It seems that, in 2d, the optimal geometries are those of sequential laminates, which are created through successive lamination, i.e., by adding layers of the pure phases, as these solve the deeper problem of completely characterizing all possible matrix-valued conductivity functions [19], but far less is known in 3d [20].

In summary, it is unknown in general whether the essential conclusion of optimality of simple laminates can be applied in the case of complex-valued material parameters. Nevertheless, we proceed by assuming the existence of a relaxed admissible design set of composite designs

$$CD := CD_{\mathbb{C}} = \left\{ (\theta, A^*) \in L^\infty(\Omega; [0,1] \times \mathbb{C}^{N\times N}) \mid A^*(x) \text{ in } \mathcal{G}_{\theta(x)} \text{ a.e. in } \Omega \right\},$$

together with an appropriate relaxed objective functional $J^* := J^*_{\mathbb{C}}(\theta, A^*)$, which make the relaxed problem well posed and enable application of the direct method of the calculus of variations in order to derive optimality criteria. In the real-valued case, $\mathcal{G}_\theta$ and the optimality of simple laminates are derived from the sequential laminates as optimal microstructures [3]. Taking into account the parallel above motivates us to assume simple rank-1 laminates as the materials of interest even in the complex-valued material parameter case.

In three dimensions, a rank-1 laminate consisting of two isotropic materials with material parameters $\alpha, \beta \in \mathbb{C}$ in proportion θ and $1-\theta$ with lamination direction $e = (1,0,0)^T$ is described by eigenvalues equal to the harmonic and arithmetic mean

(see [14]):

$$A^* = \begin{pmatrix} \lambda_\theta^- & 0 & 0 \\ 0 & \lambda_\theta^+ & 0 \\ 0 & 0 & \lambda_\theta^+ \end{pmatrix}, \tag{11a}$$

$$\text{with } \lambda_\theta^- = \left(\frac{\theta}{\alpha} + \frac{1-\theta}{\beta} \right)^{-1} \text{ and } \lambda_\theta^+ = \theta\alpha + (1-\theta)\beta. \tag{11b}$$

Simple laminates with arbitrary lamination direction e are accordingly described by rotation angles φ, ψ and density θ. Restriction of the design set to simple laminates and formulation of the derived directional derivative with regard to the admissible increments $\delta\theta, \delta\varphi$ and $\delta\psi$ forms the basis for application of a gradient descent method below.

The adapted problem formulation then reads as follows: Find $(\tilde{\theta}, \tilde{A^*})$ such that

$$(\tilde{\theta}, \tilde{A^*}) = \underset{(\theta, A^*) \in CD}{\arg\min}\ J^*(\theta, A^*), \tag{12a}$$

$$J^*(\theta, A^*) = \int_\Omega \theta(x) g_\alpha(x, u(x), \bar{u}(x)) + (1-\theta(x)) g_\beta(x, u(x), \bar{u}(x))\, \mathrm{d}x + l \int_\Omega \theta(x)\, \mathrm{d}x, \tag{12b}$$

where u is the (weak) solution of

$$\begin{cases} -\mathrm{div}(A^*(x)\nabla u(x)) = f(x), & x \in \Omega, \\ u(x) = 0, & x \in \partial\Omega, \end{cases} \tag{12c}$$

where the density θ and homogenized tensor A^* are the design variables, the relaxed objective functional depends on the density θ and the state equation is the so-called homogenized problem involving the homogenized tensor A^*. Based on this relaxed problem formulation, optimality criteria are now to be derived. For this purpose, we compute the directional derivative of the objective functional next.

4.2 Gâteaux differential of the objective functional

Computation of the directional derivative is not straightforward for objective functionals which are not only dependent on a complex variable z but also explicitly or implicitly dependent on its complex conjugate $\bar{z}$. Objective functionals of this type occur frequently in the context of signal processing (see for example [21]).

In general, the derivative with respect to a complex-valued variable cannot be evaluated directly when the function depends on the variable's conjugate, these functions are called non-analytic functions and are not complex differentiable [22]. One possibility to overcome this problem is to define the formal partial derivatives, first introduced by W. Wirtinger in [23], and to treat the variable and its complex conjugate as independent, each considered to be constant with respect to the other. A compact and clearly

arranged summary of the important aspects concerning differentials of real-valued functions having complex-valued arguments can be found in [24]. Besides the validity of common real-valued differentiation rules for sum, product, and composition of functions, a very useful property of the Wirtinger derivative is

$$\frac{\partial}{\partial z}\bar{z} = \frac{\partial}{\partial \bar{z}} z = 0,$$

which allows to treat $\bar{z}$ as constant when differentiating with respect to z and vice versa.

On the basis of this formal definition, one obtains for any real-valued function f with complex-valued argument z the differential $\mathrm{d}f$ as

$$\mathrm{d}f = 2\mathbb{R}\mathrm{e}\left\{\frac{\partial f(z)}{\partial z} dz\right\} = 2\mathbb{R}\mathrm{e}\left\{\frac{\partial f(z)}{\partial \bar{z}} d\bar{z}\right\}, \tag{13}$$

where $\mathbb{R}\mathrm{e}\{\cdot\}$ denotes the real part. Based on this, it is possible to derive the directional derivative of the objective functional. This includes introduction of the appropriately adapted adjoint problem in order to eliminate the dependence of the derivative on the state increment.

Initially, the objective functional and thus the corresponding directional derivative is, besides the dependence on the increments of the design variables $\delta\theta$ and δA^*, still dependent on the state increment δu and $\delta\bar{u}$. Introduction of the corresponding adjoint problem enables elimination of this dependency of the directional derivative on δu, respectively, $\delta\bar{u}$. This result can be achieved by using the formal Lagrange technique, as is commonly done in optimal control of partial differential equations [11]. The necessary optimality conditions are then derived by formally equating to zero the derivatives with respect to the optimization variables of the appropriately formulated Lagrangian in the complex case, see for example [25–27] for Lagrange functions with complex-valued state variables. Nevertheless, by proper definition of the adjoint problem and application of the Wirtinger calculus, determination of the Gâteaux differential of the objective functional follows the argumentation of [3] in the real-valued parameter setting. It turns out (see Appendix) that the adjoint problem is given by

$$\begin{cases} -\mathrm{div}(A^{*H}(x)\nabla p(x)) = \theta(x)\frac{\partial g_\alpha}{\partial \bar{u}}(x,u,\bar{u}) + (1-\theta(x))\frac{\partial g_\beta}{\partial \bar{u}}(x,u,\bar{u}), & x \in \Omega, \\ p(x) = 0, & x \in \partial\Omega, \end{cases} \tag{14}$$

where A^{*H} is the conjugate transpose (Hermitian transpose) of A^* and the derivatives $\frac{\partial g_\alpha}{\partial \bar{u}}(x,u,\bar{u})$ and $\frac{\partial g_\beta}{\partial \bar{u}}(x,u,\bar{u})$ must be understood as derivatives in the sense of Wirtinger calculus by differentiating with respect to the complex conjugate of u, treating u as constant.

The conditions

$$\begin{cases} \frac{\partial g_{\alpha,\beta}}{\partial \bar{u}}(x,u,\bar{u}) \text{ is measurable in } x \text{ for each fixed } u,\bar{u} \in \mathbb{C}, \\ \frac{\partial g_{\alpha,\beta}}{\partial \bar{u}}(x,u,\bar{u}) \text{ is continuous in } u,\bar{u} \text{ for each fixed } x \in \Omega, \\ |\frac{\partial g_{\alpha,\beta}}{\partial \bar{u}}(x,\bar{u})| \leq k'(x) + C'|\bar{u}|^{m-1} \text{ for } 1 \leq m < \frac{2N}{N-2} \text{ with } k'(x) \in L^q(\Omega),\ q > \frac{2N}{N-2}, \end{cases}$$

ensure differentiability of the objective functional as well as that the source term of the adjoint Eq. (14) is in $H^{-1}(\Omega)$.

The objective functional $J^*(\theta, A^*)$ is Gâteaux differentiable on the space of admissible composite designs and the directional derivative is finally given by

$$\begin{aligned} \delta J^*(\theta, A^*) = &\int_\Omega \delta\theta(x)(g_\alpha(x,u(x),\bar{u}(x)) + l - g_\beta(x,u(x),\bar{u}(x)))\,\mathrm{d}x \\ &- 2\mathbb{R}\mathrm{e}\left\{\int_\Omega \langle \delta A^*(x)\nabla u(x), \nabla p(x)\rangle\,\mathrm{d}x\right\}. \end{aligned}$$

Here, $\delta\theta$ and δA^* are admissible increments in CD, u is the (weak) solution of the state Eq. (12c) and p is the (weak) solution of the adjoint state Eq. (14). Moreover, $\langle\cdot,\cdot\rangle$ denotes the standard inner product of $\mathbb{C}^N$. For the full derivation of the formulation, see Appendix. We conclude this Section with formulating an optimization algorithm based on the gradient method.

4.3 Optimization algorithm based on simple laminates

The design parameters for an optimization routine based on the gradient method are given by the density θ and the lamination direction e of the composite, which corresponds to the two rotation angles φ and ψ of the rank-1 laminate tensor in three dimensions, see (11). An optimal tensor is thus given by

$$A^*(\theta,\psi,\varphi) = R_1(\psi)R_2(\varphi)\begin{pmatrix} \lambda_\theta^- & 0 & 0 \\ 0 & \lambda_\theta^+ & 0 \\ 0 & 0 & \lambda_\theta^+ \end{pmatrix} R_2^{-1}(\varphi)R_1^{-1}(\psi),$$

with rotation matrices

$$R_1(\psi) = \begin{pmatrix} \cos(\psi) & -\sin(\psi) & 0 \\ \sin(\psi) & \cos(\psi) & 0 \\ 0 & 0 & 1 \end{pmatrix} \quad \text{and} \quad R_2(\varphi) = \begin{pmatrix} \cos(\varphi) & 0 & \sin(\varphi) \\ 0 & 1 & 0 \\ -\sin(\varphi) & 0 & \cos(\varphi) \end{pmatrix}.$$

In what follows, we use the so-called Z–Y–X Euler angles (see [28] for details), where the position of a body-fixed frame B in space is determined by the three angles ψ_E, θ_E and φ_E. Starting with the frame B, which coincides with the spatial frame with axes x, y and z, B is first rotated about z by the angle ψ_E which transforms the frame to x', y' and $z' = z$. In a next step, B is rotated about y' by the angle θ_E providing x'', $y'' = y'$ and z'' and, in a last step, about x'' by the angle φ_E, leading to $x''' = x''$, y''' and z'''. In order to avoid confusion and since only two rotation angles are sufficient to

describe the lamination direction e, the two angles describing the lamination direction are defined by $\psi = \psi_E$ and $\varphi = \theta_E$.

The directional derivative δJ^* of the objective functional $J^*(\theta, \psi, \varphi)$ with respect to an admissible increment $(\delta\theta, \delta\psi, \delta\varphi)$ is computed as

$$\begin{aligned}\delta J^*(\theta, \psi, \varphi) = &\int_\Omega \left(\frac{\partial A^*}{\partial \psi}(x)\nabla u(x) \cdot \nabla p(x)\right) \delta\psi(x)\,\mathrm{d}x \\ &+ \int_\Omega \left(\frac{\partial A^*}{\partial \varphi}(x)\nabla u(x) \cdot \nabla p(x)\right) \delta\varphi(x)\,\mathrm{d}x \\ &+ \int_\Omega Q(x)\delta\theta\,\mathrm{d}x\end{aligned}$$

with

$$Q(x) = g_\alpha(x, u(x)) - g_\beta(x, u(x)) + l - \left(\frac{\partial A^*}{\partial \theta}(x)\nabla u(x) \cdot \nabla p(x)\right). \tag{15}$$

Thus, an optimization algorithm based on the gradient method for the iterative approximation of the solution to the given minimization problem is defined as follows.

Optimization algorithm

Initialization: Initialize θ_0, ψ_0, and φ_0 and compute A_0^*.
(For simplicity, choose constant θ_0 and constant angles ψ_0 and φ_0.)
Compute u_0 and p_0 as weak solutions of (12c) and (14).
Compute $J(\theta_0, \psi_0, \varphi_0)$.

Iteration for $k \geq 0$ until convergence:
Set $J(\theta_{k+1}, \psi_{k+1}, \varphi_{k+1}) = J(\theta_k, \psi_k, \varphi_k)$.

Until $J(\theta_{k+1}, \psi_{k+1}, \varphi_{k+1}) < J(\theta_k, \psi_k, \varphi_k)$:
Adjust stepsize t_k.

Until volume constraint fulfilled:
Adjust l_k via bisection method.
Update parameters as

$$\begin{aligned}\psi_{k+1} &= \psi_k - t_k \left(\frac{\partial A_k^*}{\partial \psi}(\theta_k, \psi_k, \varphi_k)\nabla u_k \cdot \nabla p_k\right), \\ \varphi_{k+1} &= \varphi_k - t_k \left(\frac{\partial A_k^*}{\partial \varphi}(\theta_k, \psi_k, \varphi_k)\nabla u_k \cdot \nabla p_k\right), \\ \theta_{k+1} &= \max(0, \min(1, \theta_k - t_k Q_k)),\end{aligned}$$

with Q_k defined by (15) with corresponding input values l_k, A_k^*, u_k and p_k.
Compute A_{k+1}^* and u_{k+1} and p_{k+1} as weak solutions of (12c) and (14) with design parameters θ_{k+1}, φ_{k+1} and ψ_{k+1}.
Compute $J(\theta_{k+1}, \psi_{k+1}, \varphi_{k+1})$.
Update k to $k + 1$.

In order to ensure the compliance with the volume constraint, the algorithm includes adaptation of the Lagrange multiplier performed by the inner loop adjusting l_k for every step size t_k. Following the argumentation of Allaire in [3], the bisection method is used since the volume of phase A is a non-increasing function of l.

As result of this optimization algorithm, parameters of simple laminates consisting of phases A and B in each material point, i.e., the ratio of both phases θ and the direction of the laminate layers described by the two angles ψ and φ, are provided. In order to obtain an optimal 0–1 design consisting of only pure phases A and B, the process can be combined with a penalization process that penalizes local mixtures of two materials (see [3, Chap. 5]). However, in the examples considered in the application below, the method already converges to a 0–1 design even without this penalization so that the algorithm output provides the information of the shape and position of the optimal sensor in terms of spatial points in which $\theta \approx 1$.

The described optimization method based on assumptions on existence of a relaxed design set and restriction of the design set to simple laminates is validated by a comparison to known results for the (real-valued) so-called worst conductor model next and then successfully applied to the question of optimizing the design of a capacitive sensor in connection with electromagnetic emission during fracture of brittle dielectric materials.

5 Numerical examples

In what follows, the method is tested and validated in the sense that its results are shown to tend to published ones for a well-known real-valued example as the imaginary part of one material constant approaches zero. Moreover, results for an optimal sensor design problem are presented showcasing the functioning of the method. For both examples, the gradient method for complex-valued material parameters is implemented in MATLAB, while the numerical approximation of the state u_k and adjoint state p_k is implemented within the finite element method software COMSOL Multiphysics®.

5.1 Validation of the implemented method

The implementation and functionality of the presented method with complex-valued material parameters is validated by application to the so-called worst conductor model, for which results can be found e.g., in [3, Chap. 5.1] for the two-dimensional case. In standard formulation, this self-adjoint optimization problem seeks the worst conducting/best isolating design of the two phases A and B with equal volume fractions of 50% and real-valued material parameters subjected to a uniform source term. In the published results we compare to, $\alpha = 1$ and $\beta = 2$ are chosen on a square domain $\Omega = (0, 1)^2$.

We rewrite the formulation in [3, Chap. 5.1] in order to address the problem with material parameters taking values in $\mathbb{R}$ or $\mathbb{C}$ in the same way. For given $\alpha = \alpha_\mathrm{r} + \mathrm{i}\alpha_\mathrm{i}$

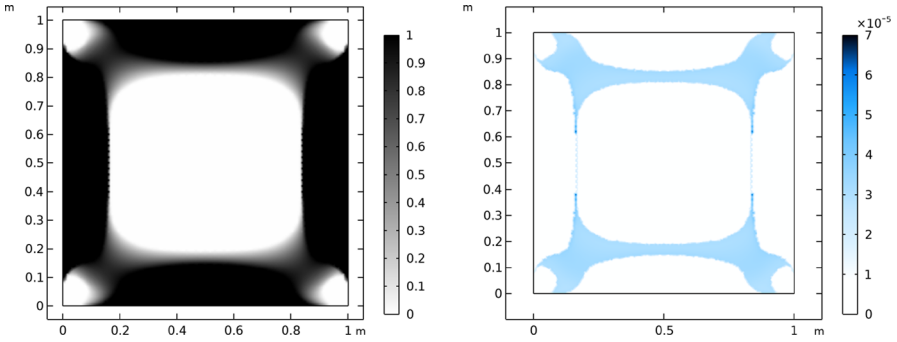

Fig. 1 Result of the optimization routine after 200 iteration steps for $\alpha_\mathrm{i} = 0.001$. Left: Density θ. Right: Difference to the result for $\alpha_\mathrm{i} = 0$, i.e., $|\theta - \theta_0|$, where θ_0 is the result for $\alpha_\mathrm{i} = 0$

and $\beta = \beta_\mathrm{r} + \mathrm{i}\beta_\mathrm{i}$ with $\alpha_\mathrm{r}, \alpha_\mathrm{i}, \beta_\mathrm{r}, \beta_\mathrm{i} \in \mathbb{R}$, we seek to minimize

$$\min_{(\theta, A^*) \in CD} J^*(\theta, A^*) = \min_{(\theta, A^*) \in CD} -\int_\Omega \frac{1}{2}(u + \bar{u})\,\mathrm{d}x + l \int_\Omega \theta(x)\,\mathrm{d}x, \tag{16}$$

subject to u being the solution of

$$\begin{cases} -\mathrm{div}(A^*(x)\nabla u(x)) = 1, & x \in \Omega, \\ u(x) = 0, & x \in \partial\Omega. \end{cases} \tag{17}$$

In order to validate our method and implementation, we consider a sequence of optimization problems with $\beta = 2$ and $\alpha = 1 + \mathrm{i}\alpha_\mathrm{i}$ with decreasing imaginary part, i.e., $\alpha_\mathrm{i} = 0.1$, $\alpha_\mathrm{i} = 0.01$ and $\alpha_\mathrm{i} = 0.001$, and compare the results to those of the published results for $\alpha_\mathrm{i} = 0$ in order to analyze the behavior of the design results as the problem approaches the purely real-valued case.

The optimization routine is initialized with constant density $\theta = 0.5$ and constant lamination direction $e = (1, 0)^T$. The use of quadratic Lagrange elements on a triangular mesh resulting in 12 765 DOF proved to be sufficient. In contrast to the optimization method based on optimality conditions conducted in [3], where 50 iteration steps are sufficient to obtain a converged value of the objective functional, the gradient method required 200 steps.

Figure 1 shows the optimized design in terms of the design parameter θ for $\alpha = 1 + 0.001\mathrm{i}$ (left) and the difference to the result for $\alpha = 1$, i.e., $|\theta - \theta_0|$, where θ_0 is the result for $\alpha = 1$. The optimized design looks virtually identical to that given by [3, Chap. 5.1], which validates our implementation in this sense.

Figure 2 compares designs θ to the real-valued result θ_0 for decreasing imaginary parts α_i of the material parameter, i.e., it shows the L^2-Norm of the difference of the optimized designs to θ_0. For successively smaller imaginary parts, the optimized designs converge to the design for the real-valued case, i.e., $\alpha_\mathrm{i} = 0$.

On the basis of this validation, the method is now applied to the problem of optimizing the design of an electromagnetic sensor.

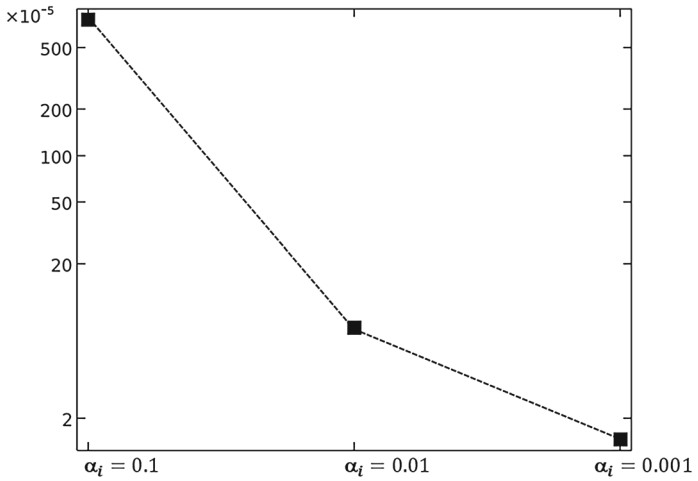

Fig. 2 L^2-Norm of the difference to the real-valued case for simulations with different imaginary parts of the material parameter α

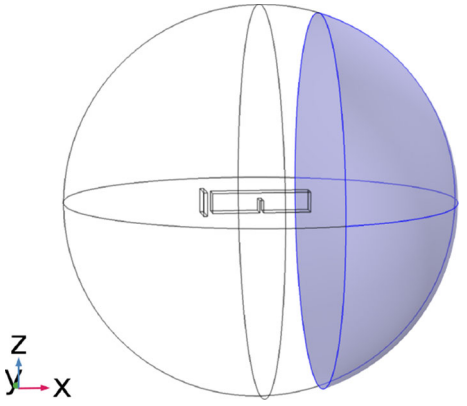

Fig. 3 Geometric arrangement of the model. Domain Ω (sphere) with single-edge notched specimen in the middle and grounded sensor part to the left of the specimen. The optimization domain, where the measuring sensor part is to be placed, (Ω_1) is shown in blue

5.2 Application to optimal sensor design

The application example presented in what follows is based on an experiment designed to investigate electromagnetic emission during mode-I fracture of brittle dielectric materials in three-point bending tests of single-edge notched specimen (see [29] for further details). In the original experimental setup, the geometric arrangement of which is shown in Fig. 3 neglecting the universal testing machine exerting a vertical force on the top surface of the specimen, the electric potential emerging during fracture of the specimen is measured by a capacitive sensor which consists of two copper plates: one plate (the left one in Fig. 3) is grounded while the other plate (the right one, which is to be designed) is attached to a circuit measuring the occurring electric potential. The presented investigation is inspired by the question of optimized position and shape of the measuring non-grounded sensor part. Evaluation of the experiments show a

dipole behavior of the emitting source [29], which can be modeled by oppositely applied charge densities on two hypothetical crack surfaces in the specimen. For a given source on the two hypothetical crack surfaces, the aim is to place a sensor of material A in the given subdomain Ω_1 (shown in blue in Fig. 3) in such a way that the maximum energy in the sensor is captured at the dominant emitted frequency.

The parameter describing the material properties derived in Sect. 2.3 represents a joint parameter of electric permittivity and conductivity for given frequency $\omega \neq 0$. Hence, in what follows, the two materials A and B with material parameters α and β are distinguished phenomenologically in terms of their ability to absorb the electric field, which is reflected in different imaginary parts of the material parameter. This approach is based on the assumption that a sensor made of material A (e.g., copper) has significantly stronger capability for absorption compared to the surrounding material B (e.g., air).

The aim is the solution to the optimization problem searching for the sensor design maximizing the energy measured at a sensor built of material A within the subdomain Ω_1. The following choice of objective functional serves as a proxy for the captured (absorbed) energy. We aim to minimize

$$\min_{(\theta, A^*) \in CD} J^*(\theta, A^*) = \min_{(\theta, A^*) \in CD} - \int_{\Omega_1} \theta(x)(u(x)\bar{u}(x))\,\mathrm{d}x + l \int_{\Omega_1} \theta(x)\,\mathrm{d}x$$

on a subdomain Ω_1 subject to the electric potential u satisfying the complex-valued state equation

$$\begin{cases} -\operatorname{div}(A^*(x)\nabla u(x)) = F, & x \in \Omega, \\ u(x) = 0, & x \in \partial\Omega. \end{cases}$$

The vanishing Dirichlet boundary conditions model a grounded encasing at the boundary of the domain or an attenuated far field far away from the region of interest.

To showcase the functioning of the method, material parameters $\alpha = 1 + 2\mathrm{i}$, $\beta = 1 + 1\mathrm{i}$ and a volume constraint of 20% are chosen, the material parameter in Ω_2 equals $\beta = 1 + 1\mathrm{i}$ and the source is given with strength of 100 and -100 on the two hypothetical crack surfaces, respectively. Since the study is focused on qualitative results, no units are given here and in what follows.

In order to reduce computational cost, the domain Ω is numerically truncated by a so-called infinite element domain Ω_{ied}, which surrounds the design area of interest. This approach has proven effective for the restriction of the model to parts of the geometry which contain necessary details. When using the infinite element domain, there must not be changes of material parameters at the boundary adjoining the infinite element domain. For this reason, a material buffer zone Ω_{b} is introduced in the model in which no optimization takes place. Both Ω_{ied} and Ω_{b} are occupied by phase B, their geometric arrangement is illustrated in Fig. 4. In what follows, reference to an "optimal design" is always reference to the improved design after the application of the optimization routine.

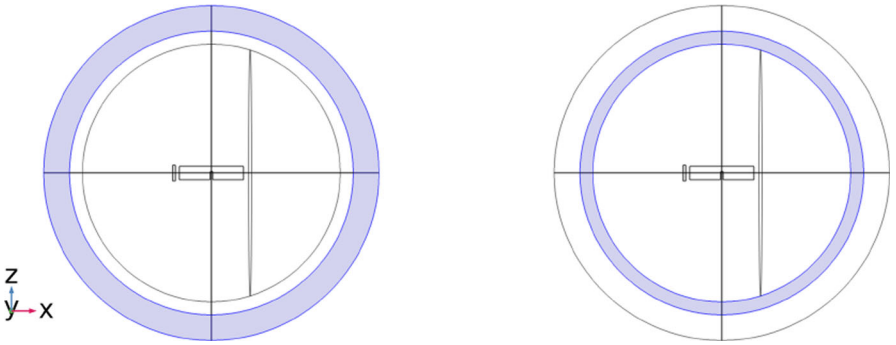

Fig. 4 Geometric arrangement of the model illustrated in z–x-cut-plane. Left: infinite element domain Ω_{ied} (blue). Right: material buffer zone Ω_{b} (blue)

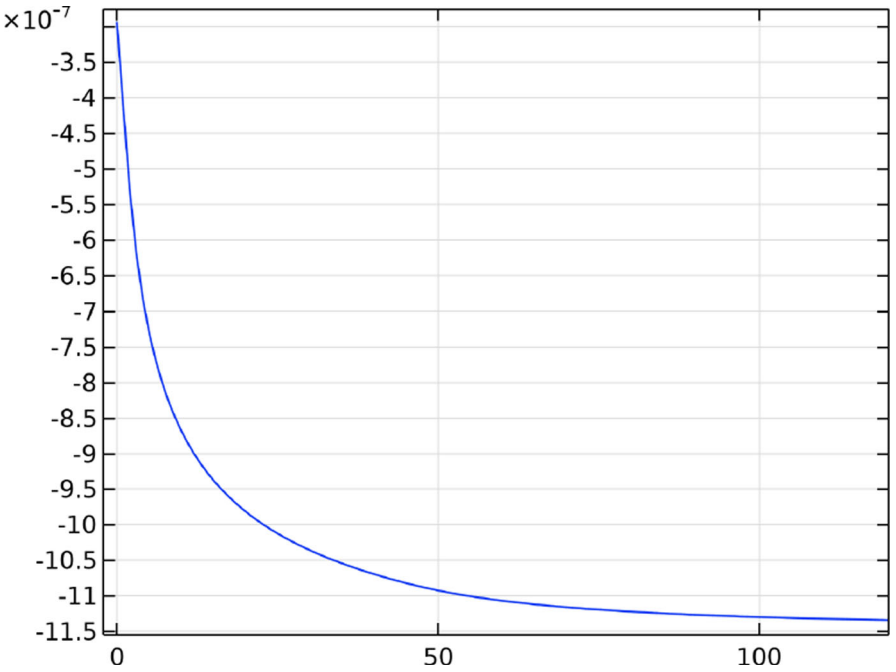

Fig. 5 Development of the value of the objective functional over 120 steps of the optimization routine

Numerical approximation of the state u_k and adjoint state p_k is performed using the finite element method on a triangular mesh with quadratic Lagrange elements resulting in 76 000 DOF, initialized with constant density $\theta = 0.2$ and constant lamination direction $e = (1, 0, 0)^T$. Figures 5, 6 and 7 illustrate the progress of the gradient method for the first 120 steps of the described optimization problem in the area of interest without infinite element domain.

The plot of the objective functional in Fig. 5 shows a significant improvement of the objective functional with converging behavior. The major part of the optimization

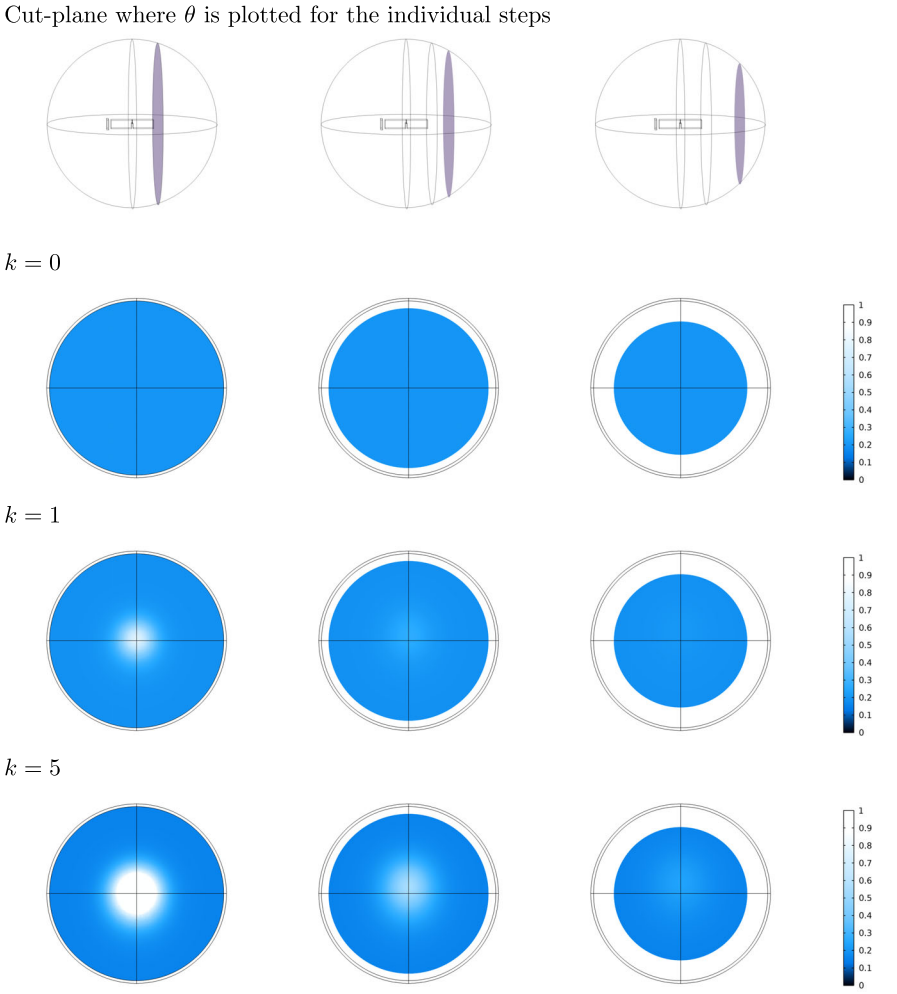

Fig. 6 Progress of the gradient method. Density θ at initialization ($k = 0$) and after steps $k = 1$ and $k = 5$ in different cut-planes of Ω_1

takes place approximately within the first 60 steps of the algorithm, which is further supported by Figs. 6 and 7; after 60 steps of the gradient method, a design has emerged, which consists mostly of a 0–1-design of the pure phases A and B with only a small transition region with laminate materials described by intermediate densities $\theta \in (0, 1)$. Figure 7 shows that this transition zone decreases further in size until step 120, at which the optimization routine terminates. It is likely that further optimization steps will lead to continuous reduction of this transition zone until ultimately a clear 0–1 design is achieved. Due to the fact that the specimen is positioned in the middle of the sphere, the hypothetical crack surfaces are asymmetrically positioned in the sphere (not in the sphere center but shifted upwards in z-direction). This is reflected

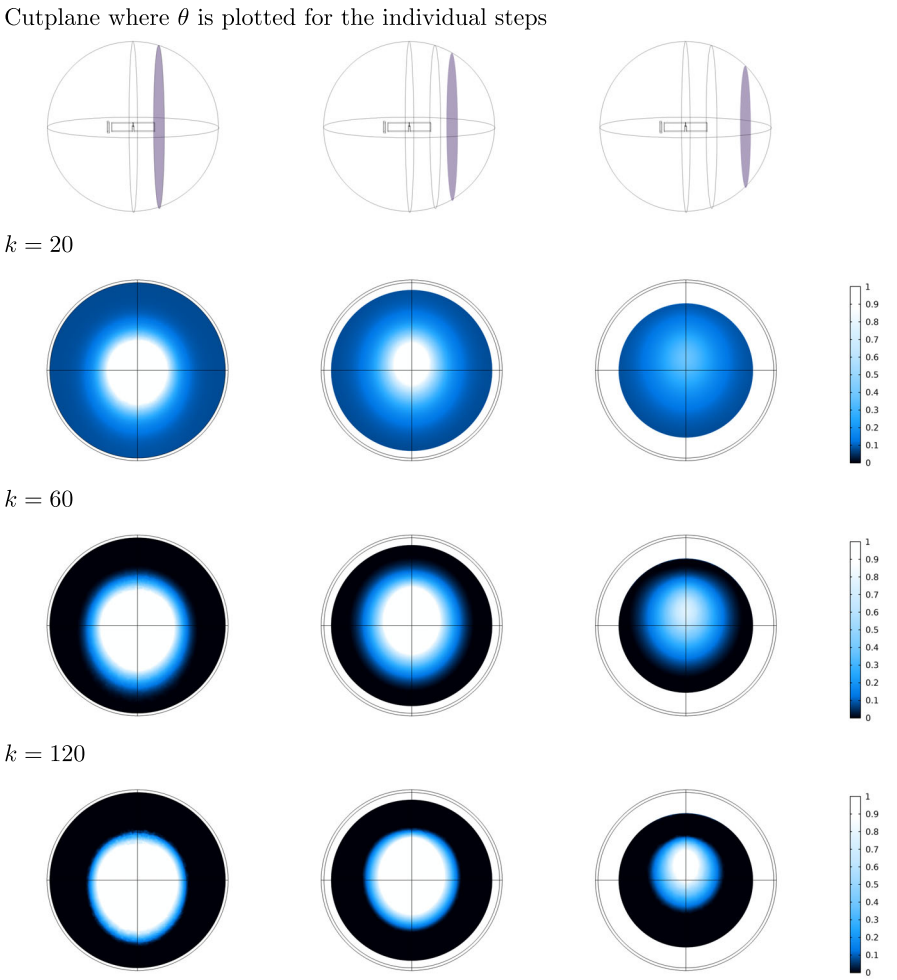

Fig. 7 Progress of the gradient method. Density θ after steps $k = 20$, $k = 60$ and $k = 120$ in different cut-planes of Ω_1

in the emerged sensor design, which also shows asymmetric behavior regarding the x–y-cut-plane.

The application example demonstrates that the objective functional can be significantly improved by use of the derived gradient method. The optimized sensor design reflects asymmetries of the source and geometrical arrangement. Furthermore, it becomes clear that, just as in typical applications with real-valued material parameters, no subsequent penalty process is necessary since a 0–1-design is already formed in the optimization procedure. In further studies of the application, it became apparent that an adjustment of the source strength depending on the geometry is advantageous in order to improve feasibility of the method. In particular, a stronger source leads to faster convergence to the desired design in the considered example.

6 Conclusion

For two-phase design optimization problems subject to a scalar second-order elliptic equations with complex-valued material parameters, application of the relaxation by homogenization method described in [3] for real-valued parameters values requires several extensions. Making assumptions on the admissible design set, which are known to hold in the real-valued case but remain an open question in the complex-valued case, we derive the Gâteaux differential of the objective functional using Wirtinger calculus and devise an optimization method based on the restriction of the design set to simple laminates. Numerical simulations based on the resulting method show that it successfully optimizes complex-valued design problems.

Appendix

Derivation of the directional derivative of the objective functional

In order to derive the formulation of the directional derivative of the objective functional, consider the objective functional $J^*(\theta, A^*)$, which is formally still dependent on the state u and the complex conjugate of the state $\bar{u}$. Thereby, we define $\theta[t](x) := \theta(x) + t\delta\theta(x)$ with admissible increment $\delta\theta \in L^\infty(\Omega)$ for a.e. $x \in \Omega$; $A^*[t]$, $u[t]$ and $\bar{u}[t]$ are defined correspondingly. Then,

$$\begin{aligned}\delta J^*(\theta, A^*) &= \frac{\mathrm{d}}{\mathrm{d}t} J^*(\theta[t], A^*[t], u[t], \bar{u}[t])\Big|_{t=0} \\ &= \frac{\mathrm{d}}{\mathrm{d}t}\left[\int_\Omega \theta[t] g_\alpha(x, u[t], \bar{u}[t]) + (1-\theta[t]) g_\beta(x, u[t], \bar{u}[t])\,\mathrm{d}x + l\int_\Omega \theta[t]\,\mathrm{d}x\right]\Big|_{t=0}.\end{aligned}$$

Applying Wirtinger calculus along with (13), we obtain

$$\begin{aligned}\delta J^*(\theta, A^*) = &\int_\Omega \delta\theta(x)\Big(g_\alpha(x, u(x), \bar{u}(x)) - g_\beta(x, u(x), \bar{u}(x)) + l\Big)\,\mathrm{d}x \\ &+ 2\mathbb{R}\mathrm{e}\left\{\int_\Omega \left(\theta(x)\frac{\partial g_\alpha}{\partial \bar{u}}(x, u(x), \bar{u}(x)) + (1-\theta(x))\frac{\partial g_\beta}{\partial \bar{u}}(x, u(x), \bar{u}(x))\right)\delta\bar{u}(x)\,\mathrm{d}x\right\},\end{aligned}$$

where the derivatives $\frac{\partial g_\alpha}{\partial \bar{u}}(x, u, \bar{u})$ and $\frac{\partial g_\beta}{\partial \bar{u}}(x, u, \bar{u})$ are to be understood as Wirtinger derivatives.

It remains to show

$$\begin{aligned}2\mathbb{R}\mathrm{e}\left\{\int_\Omega \left(\theta(x)\frac{\partial g_\alpha}{\partial \bar{u}}(x, u(x), \bar{u}(x)) + (1-\theta(x))\frac{\partial g_\beta}{\partial \bar{u}}(x, u(x), \bar{u}(x))\right)\delta\bar{u}(x)\,\mathrm{d}x\right\} \\ = -2\mathbb{R}\mathrm{e}\left\{\int_\Omega \langle \delta A^{*H}(x)\nabla u(x), \nabla p(x)\rangle\,\mathrm{d}x\right\}\end{aligned}$$

to eliminate the state increment in the directional derivative.

Differentiating the state equation, we obtain δu as unique solution of

$$\begin{cases} -\operatorname{div}(A^*(x)\nabla\delta u(x)) = \operatorname{div}(\delta A^*(x)\nabla u(x)), & x \in \Omega, \\ \delta u(x) = 0, & x \in \partial\Omega. \end{cases} \tag{18}$$

Multiplying Eq. (18) by $\bar{p}$, integrating by parts and noting the homogeneous Dirichlet boundary conditions, we obtain for the left-hand side

$$-\int_\Omega \langle \operatorname{div}(A^*(x)\nabla\delta u(x)),\, p(x)\rangle \,\mathrm{d}x = \int_\Omega \langle A^*(x)\nabla\delta u(x),\, \nabla p(x)\rangle \,\mathrm{d}x,$$

and for the right-hand side

$$\int_\Omega \langle \operatorname{div}(\delta A^*(x)\nabla u(x)),\, p(x)\rangle \,\mathrm{d}x = -\int_\Omega \langle \delta A^*(x)\nabla u(x),\, \nabla p(x)\rangle \,\mathrm{d}x.$$

Combination of both results leads to

$$\int_\Omega \langle A^*(x)\nabla\delta u(x),\, \nabla p(x)\rangle \,\mathrm{d}x = -\int_\Omega \langle \delta A^*(x)\nabla u(x),\, \nabla p(x)\rangle \,\mathrm{d}x. \tag{19}$$

Multiplying the adjoint Eq. (14) by $\overline{\delta u}$ and integrating by parts gives, again noting the homogeneous Dirichlet boundary condition, we obtain

$$\begin{aligned} &\int_\Omega \langle A^{*H}(x)\nabla p(x),\, \nabla\delta u(x)\rangle \,\mathrm{d}x \\ &\quad = \int_\Omega \langle \theta(x)\frac{\partial g_\alpha}{\partial \bar{u}}(x, u(x), \bar{u}(x)) \\ &\qquad + (1-\theta(x))\frac{\partial g_\beta}{\partial \bar{u}}(x, u(x), \bar{u}(x)),\, \delta u(x)\rangle \,\mathrm{d}x. \end{aligned} \tag{20}$$

Considering

$$\begin{aligned} \int_\Omega \langle A^{*H}(x)\nabla p(x),\, \nabla\delta u(x)\rangle \,\mathrm{d}x &= \int_\Omega \langle \nabla p(x),\, A^*(x)\nabla\delta u(x)\rangle \,\mathrm{d}x \\ &= \int_\Omega \overline{\langle A^*(x)\nabla\delta u(x),\, \nabla p(x)\rangle} \,\mathrm{d}x, \end{aligned}$$

and combination of (19) and (20) leads to

$$\begin{aligned} &\int_\Omega \langle \theta(x)\frac{\partial g_\alpha}{\partial \bar{u}}(x, u(x), \bar{u}(x)) + (1-\theta(x))\frac{\partial g_\beta}{\partial \bar{u}}(x, u(x), \bar{u}(x)),\, \delta u(x)\rangle \,\mathrm{d}x \\ &\qquad = -\int_\Omega \overline{\langle \delta A^*(x)\nabla u(x),\, \nabla p(x)\rangle} \,\mathrm{d}x, \end{aligned}$$

finally resulting in

$$2\mathbb{R}\mathrm{e}\left\{\int_\Omega \langle \theta(x)\frac{\partial g_\alpha}{\partial \bar{u}}(x,u(x),\bar{u}(x)) + (1-\theta(x))\frac{\partial g_\beta}{\partial \bar{u}}(x,u(x),\bar{u}(x)),\delta u(x)\rangle\,\mathrm{d}x\right\} = -2\mathbb{R}\mathrm{e}\left\{\int_\Omega \langle \delta A^*(x)\nabla u(x),\nabla p(x)\rangle\,\mathrm{d}x\right\},$$

which completes the derivation.

Acknowledgements The authors thank S. O. Gade and M. G. R. Sause for fruitful discussions on the electromagnetic emission problem and A. Cherkaev and G. W. Milton for helpful correspondence on the G-closure problem.

Author contributions U.W.: conceptualization, formal analysis, methodology, software; M.A.P.: conceptualization, formal analysis, methodology; Both authors contributed to writing and final editing of the manuscript.

Funding Open Access funding enabled and organized by Projekt DEAL. Open Access funding enabled and organized by Projekt DEAL. No funding was received to assist with the preparation of this manuscript.

Data availability No datasets were generated or analyzed during the current study.

Declarations

Conflict of interest The authors declare no conflict of interest.

References

1. Bendsœ MP (1995) Optimization of structural topology, shape and material. Springer, Berlin, Heidelberg
2. Deaton JD, Grandhi RV (2014) A survey of structural and multidisciplinary continuum topology optimization: post 2000. Struct Multidiscip Optim 49:1–38
3. Allaire G (2002) Shape optimization by the homogenization method. Springer, New York
4. Sigmund O, Maute K (2013) Topology optimization approaches - a comparative review. Struct Multidiscip Optim 48:1031–1055
5. Tartar L (2009) The general theory of homogenization. Springer, Berlin, Heidelberg
6. Bartelmann M, Feuerbacher B, Krüger T, Lüst D, Rebhan A, Wipf A (2018) Theoretische Physik 2 Elektrodynamik. Springer, Berlin
7. Orfanidis SJ (2016) Electromagnetic waves and antennas. Rutgers University
8. Jackson JD (2006) Klassische Elektrodynamik, 4 überarbeitete. Walter de Gruyter, Berlin
9. Showalter RE (1997) Monotone operators in Banach space and nonlinear partial differential equations, vol 49. American Mathematical Society
10. Alt HW (2012) Lineare Funktionalanalysis. Springer, Berlin, Heidelberg

11. Tröltzsch F (2009) Optimale Steuerung partieller Differentialgleichungen. Vieweg+Teubner, Wiesbaden
12. Murat F, Tartar L (2018) H-Convergence. In: Cherkaev AV, Kohn R (eds) Topics in the mathematical modelling of composite materials. Springer, Cham, pp 21–43
13. Tartar L (2000) An introduction to the homogenization method in optimal design. Optimal shape design: lectures given at the joint C.I.M., C.I.M.E. Summer school held in Tróia, Portugal, June 1–6, 1998, 47–156. Springer, Berlin, Heidelberg
14. Milton GW (2002) The theory of composites. Cambridge University Press, Cambridge
15. Gibiansky LV (1993) Bounds on the effective moduli of composite materials. School on Homogenization ICTP, Trieste, September 6–17
16. Cherkaev A (2000) Variational methods for structural optimization. Springer, Berlin-Heidelberg
17. Cherkaev A, Gibiansky LV (1992) The exact coupled bounds for effective tensors of electrical and magnetic properties of two-component two-dimensional composites. Proc R Soc Edinburgh Sect A Math 122(1–2):93–125
18. Clark KE, Milton GW (1993) Optimal bounds correlating electric, magnetic and thermal properties of two-phase, two-dimensional composites. Proc R Soc Lond Ser A Math Phys Sci 448:161–190
19. Milton GW (1986) A proof that laminates generate all possible effective conductivity functions of two-dimensional, two-phase media. In: Papanicolaou G (ed) Advances in multiphase flow and related problems: proceedings of the workshop on cross disciplinary research in multiphase flow, Leesburg, Virginia, June 2–4, 1986. SIAM
20. Kern C, Miller OD, Milton GW (2020) Tight bounds on the effective complex permittivity of isotropic composites and related problems. Phys Rev Appl 14(5):054068
21. Johnson DH, Dudgeon DE (1993) Array signal processing: concepts and techniques. PRT Prentice-Hall Inc, Englewood Cliffs, New Jersey
22. Rudin W (1986) Real and complex analysis. McGraw-Hill, New York
23. Wirtinger W (1926) Zur formalen Theorie der Funktionen von mehr komplexen Veränderlichen. Math Ann 97:357–375
24. Hunger R (2007) An introduction to complex differentials and complex differentiability. Technical Report TUM-LNS-TR-07-06, TUM
25. Agrawal A, Hoppe RHW (2017) Optimization of plane wave directions in plane wave discontinous Galerkin methods for the Helmholtz equation. Port Math 74:69–89
26. von Winckel G, Borzì A, Volkwein S (2009) A globalized Newton method for the accurate solution of a dipole quantum control problem. SIAM J Sci Comput 31(6):4176–4203
27. von Winckel G, Borzì A (2008) Computational techniques for a quantum control problem with H^1-cost. Inverse Prob 24:034007
28. Craig J (1986) Introduction to robotics mechanics and control. Addison-Wesley publishing company
29. Gade SO, Weiss U, Peter MA, Sause MGR (2014) Relation of electromagnetic emission and crack dynamics in epoxy resin materials. J Nondestruct Eval 33:711–723